PCCP

Accepted Manuscript




ROYAL SOCIETY OF CHEMISTRY

www.rsc.org/pccp

# A Broken-Symmetry Density Functional Study of Structures, Energies, and Protonation States along the Catalytic O-O Bond Cleavage Pathway in *ba*$_3$ Cytochrome *c* Oxidase from *Thermus thermophilus*

**Wen-Ge Han Du,[†] Andreas W. Götz,[‡] Longhua Yang,[⊤,‡] Ross C. Walker[‡,⊥] and Louis Noodleman[†,*]**

[†] Department of Integrative Structural and Computational Biology, GAC1118, The Scripps Research Institute, 10550 North Torrey Pines Road, La Jolla, CA 92037.

[‡] San Diego Supercomputer Center, University of California San Diego, 9500 Gilman Drive MC0505, La Jolla, CA 92093.

[⊤] Institute for Advanced Study and Department of Chemistry, Nanchang University, 999 Xufudadao, Nanjing, Jiangxi 330031, China

[⊥] Department of Chemistry and Biochemistry, University of California San Diego, 9500 Gilman Drive MC0505, La Jolla, CA 92093.

*To whom correspondence should be addressed.
E-mail: lou@scripps.edu.
Tel: (858) 784-2840.

## ABSTRACT

Broken-Symmetry density functional calculations have been performed on the [$Fe_{a3}$, $Cu_B$] dinuclear center (DNC) of $ba_3$ cytochrome *c* oxidase from *Thermus thermophilus* in the states of [$Fe_{a3}^{3+}$-$(HO_2)^-$-$Cu_B^{2+}$, $Tyr237^-$] and [$Fe_{a3}^{4+}$=$O^{2-}$, $OH^-$-$Cu_B^{2+}$, $Tyr237^\bullet$], using both PW91-D3 and OLYP-D3 functionals. Tyr237 is a special tyrosine cross-linked to His233, a ligand of $Cu_B$. The calculations have shown that the DNC in these states strongly favors protonation of His376, which is above propionate-A, but not of the carboxylate group of propionate-A. The energies of the structures obtained by constrained geometry optimizations along the O-O bond cleavage pathway between [$Fe_{a3}^{3+}$-$(O\text{-}OH)^-$-$Cu_B^{2+}$, $Tyr237^-$] and [$Fe_{a3}^{4+}$=$O^{2-}\cdots HO^-$-$Cu_B^{2+}$, $Tyr237^\bullet$] have also been calculated. The transition of [$Fe_{a3}^{3+}$-$(O\text{-}OH)^-$-$Cu_B^{2+}$, $Tyr237^-$] → [$Fe_{a3}^{4+}$=$O^{2-}\cdots HO^-$-$Cu_B^{2+}$, $Tyr237^\bullet$] shows a very small barrier, which is less than 3.0/2.0 kcal $mol^{-1}$ in PW91-D3/OLYP-D3 calculations. The protonation state of His376 does not affect this O-O cleavage barrier. The rate limiting step of the transition from state **A** (in which $O_2$ binds with $Fe_{a3}^{2+}$) to state $\mathbf{P_M}$ ([$Fe_{a3}^{4+}$=$O^{2-}$, $OH^-$-$Cu_B^{2+}$, $Tyr237^\bullet$], where O-O bond is cleaved) in the catalytic cycle is, therefore, the proton transfer originating from Tyr237 to O-O to form the hydroperoxo [$Fe_{a3}^{3+}$-$(O\text{-}OH)^-$-$Cu_B^{2+}$, $Tyr237^-$] state. The importance of His376 in proton uptake and the function of propionate-A/neutral-Asp372 as a gate to prevent the proton from back-flowing to the DNC are also shown.

# Introduction

Cytochrome *c* oxidase (C*c*O) is the terminal enzyme of the respiratory chain in the inner mitochondrial membrane of eukaryotes or alternatively in the periplasmic membrane in aerobic bacteria. It reduces $O_2$ to $H_2O$ and pumps protons across the membrane to create the chemiosmotic proton gradient.[1-4] The catalytic site of C*c*O which binds and reduces $O_2$ by $4e^-/4H^+$ transfer contains a heme $a_3$ ($Fe_{a3}$) and a Cu ion ($Cu_B$) — forming the dinuclear (or binuclear) center (DNC or BNC). $Cu_B$ is in the proximity (~5 Å) of $Fe_{a3}$.[5-15] Further, a C*c*O protein contains another two redox centers: a homodinuclear Cu dimer ($Cu_A$) which serves as the initial site of electron entry to C*c*O,[16,17] and another heme, which is heme A ($Fe_a$) in the case of *aa₃* type of C*c*O, or heme B ($Fe_b$) in *ba₃* type of C*c*O. The structures and components of the DNC's in *aa₃* and *ba₃* types of C*c*O's are very similar.[10-15] The DNC observed in the X-ray crystal structure (pdb code: 3S8G, 1.7 Å resolution)[15] of *ba₃* C*c*O from *Thermus thermophilus* (*Tt*) is shown in Figure 1. The $Fe_{a3}$ site has one histidine ligand (His384) and $Cu_B$ has three histidine ligands: His233, His282, and His283. His233 covalently links with the Tyr237 side chain. This linkage is common to all C*c*O's but otherwise unknown in metalloenzymes. There is a water cluster above the DNC. The interstitial water molecules in C*c*O are probably involved in catalysis by assisting proton transfer and proton pumping, and by providing a water pool and mobile pathway for the product $H_2O$ ($2H_2O$ molecules per catalytic cycle).[12] The water molecules (in 3S8G)[15] and the H-bonding residues above the DNC included in our quantum calculation models are shown in Figure 2. HOH609, the two heme propionate carboxylate groups (Prop-A and Prop-D), and part of the His283 side chain are presented in both Figures 1 and 2, in order to show how the two figures are connected. In 3S8G, the water molecule HOH609 has hydrogen bonding interactions with both propionate carboxylate groups, with HOH607, and also with the His283 side chain. Similarly positioned water molecules were also

found in other C*c*O X-ray crystal structures.[6,10-13] During the catalytic cycle, protons enter the reaction chamber through the K-path that ends at Tyr237, and exit from the region above the two propionate side chains of the $a_3$-heme into the water cluster.[18,19]

When the DNC is in the reduced state (state **R**), the molecular $O_2$ binds with $Fe_{a3}^{2+}$ and forms a formally $Fe_{a3}^{3+}$-$O_2^{-}$···$Cu_B^{+}$ state,[20-22] which is called state (intermediate) **A**.[23] The next observed state is called $\mathbf{P_M}$, which is however, not a peroxide-containing compound (as implied in the notation), but one in which the dioxygen O-O bond has already been cleaved.[24-28] Four electrons are needed to transfer to $O_2$ for the O-O bond cleavage. Now it is well established that, among the four electrons, two are from the $Fe_{a3}$ site ($Fe_{a3}^{2+} \rightarrow Fe_{a3}^{4+}$), one is from $Cu_B$ ($Cu_B^{+} \rightarrow Cu_B^{2+}$), and the 4$^{th}$ is from the unique cross-linked tyrosine ($Tyr237^{-} \rightarrow Tyr237^{\bullet}$ radical).[29,30] Therefore, the $\mathbf{P_M}$ state can be represented as [$Fe_{a3}^{4+}$=$O^{2-}$, $OH^{-}$-$Cu_B^{2+}$, $Tyr237^{\bullet}$]. Although no stable intermediate states between **A** and $\mathbf{P_M}$ are observed, it is generally believed that a bridging ferric-hydroperoxide state [$Fe_{a3}^{3+}$-$(HO_2)^{-}$-$Cu_B^{2+}$, $Tyr237^{-}$] has to be formed before the O-O bond cleavage, and the proton in the bridging $OOH^{-}$ originates from the unique cross-linked tyrosine.[2,31] Correspondingly, heme-$O_2^{2-}$-$Cu^{2+}$ synthetic compounds have been obtained,[32-35] and feasible **A** → $\mathbf{P_M}$ pathways and intermediate states have been studied theoretically.[17,36-40]

Using density functional theory (DFT) with the B3LYP potential,[41-43] Blomberg *et al*. calculated the activation energy for cleaving the O-O bond in C*c*O starting from a peroxide type structure, and compared the calculated activation energies with the observed life time of compound **A** in $aa_3$ type C*c*O, which was given as 200 μs (equivalent to 12.4 kcal mol$^{-1}$ based on transition state theory).[39] Their calculations indicate that simultaneous transfer of an electron and a proton from the tyrosine to dioxygen during bond cleavage leads to a barrier more than 10 kcal mol$^{-1}$ higher than the experimental value. They further found that an "extra" proton in the DNC would

lower the calculated activation energy by ~9 kcal $mol^{-1}$.[39] In that model, it was assumed that an extra proton was on the heme-$a_3$ farnesyl hydroxyl group, which has H-bonding interaction with the cross-linked tyrosine side chain. When the tyrosine donated a proton to $Fe^{3+}$-O-$O^-$ (state **A**), the protonated farnesyl hydroxyl group (-$OH_2$) then transferred a proton to the tyrosine. However, in such a model, their calculations showed that upon further increase of the O-O bond length, the energy of the product state went up. The tyrosine radical could not be produced, and instead, the electron needed for the O-O bond cleavage was taken from the porphyrin ring. Therefore, in order to obtain the stable tyrosine radical, this tyrosine should be in the deprotonated form in the hydroperoxo state.

In this paper, beginning with a proton transfer from the special tyrosine (Tyr237) to the dioxygen, we construct the DNC models in the hydroperoxo [$Fe_{a3}^{3+}$-$(HO_2)^-$-$Cu_B^{2+}$, $Tyr237^-$] state based on the X-ray crystal structure 3S8G of $ba_3$ C*c*O from *Tt*, and study the O-O bond breaking barrier of the transition from [$Fe_{a3}^{3+}$-$(HO_2)^-$-$Cu_B^{2+}$, $Tyr237^-$] to state $\mathbf{P_M}$ [$Fe_{a3}^{4+}$=$O^{2-}$, $OH^-$-$Cu_B^{2+}$, $Tyr237^{\bullet}$] using DFT PW91[44] and OLYP[45,46] potentials with Grimme's dispersion corrections (D3).[47] Kinetic analysis of time-resolved optical absorption experiments revealed that the $\mathbf{A} \rightarrow \mathbf{P_M}$ process in $ba_3$ C*c*O from *Tt* was only 4.8 μs (equivalent to 10.2 kcal $mol^{-1}$ based on transition state theory),[48] which is faster than in the bovine $aa_3$ system. This 10.2 kcal $mol^{-1}$ energy includes the cost to generate the hydroperoxide complex from the neutral Tyr237 by proton transfer ($\mathbf{A} \rightarrow$ [$Fe_{a3}^{3+}$-$(HO_2)^-$-$Cu_B^{2+}$, $Tyr237^-$]) and the energy barrier of the O-O cleavage in [$Fe_{a3}^{3+}$-( $HO_2)^-$-$Cu_B^{2+}$, $Tyr237^-$] $\rightarrow \mathbf{P_M}$ transition.

An extra "proton", which was found to lower the O-O cleavage energy in Ref. 39, could instead be the proton at the proton loading site (PLS) near the DNC. It is still not certain where exactly the PLS resides in $ba_3$ C*c*O's. Fee *et al.*[17] put an extra proton on top of the His376 side

chain (see Fig. 2) to represent the protonated PLS in their *ba*$_3$ DNC model for the reaction cycle calculations. On the other hand, molecular dynamics simulations and continuum electrostatic calculations performed by Kaila *et al*. indicated that the carboxylate group of Prop-A could act as a PLS.[49] We will therefore analyze whether His376 or Prop-A can hold the "extra" proton, and whether the "extra" proton in the system lowers the O-O bond cleavage barrier.

## Models and Compuational Methods

The initial Cartesian coordinates of the $Fe_{a3}^{3+}$-$(HO_2)^-$-$Cu_B^{2+}$, Tyr237$^-$ and $Fe_{a3}^{4+}$=$O^{2-}$, $OH^-$-$Cu_B^{2+}$, Tyr237$^\bullet$ DNC structures in our calculations are taken from the X-ray crystal structure 3S8G.[15] A dioxygen species (O1-O2), which was proposed as $HO_2^-$ based on our DFT calculations,[50] was observed between $Fe_{a3}$ and $Cu_B$ in this radiolyticly reduced X-ray structure. This $HO_2^-$ likely comes from the recombination of two radiation produced $HO^\bullet$ radicals formed either very near to or even in the space between the two metals of the DNC during irradiation.[15] The radiolyticly reduced structure is "off" the catalytic pathway, but still provides a very useful starting point for constructing and optimizing "on pathway" intermediates, particularly peroxo- and hydroperoxo-intermediates (see states **4**, $\mathbf{5_2}$, **5**, $\mathbf{6_2}$, and **6** in Ref 40). The size of our quantum DNC model (204/205 atoms) is basically the combination of figures 1 and 2, with different protonation states of the His376 side chain and the carboxylate group of Prop-A. The total charge of the system is zero (204 atoms) when His376 is neutral and the carboxylate group of Prop-A is not protonated, and is 1 (205 atoms) when His376 or Prop-A is protonated. The details of the oxygen components between the $Fe_{a3}^{3+/4+}$ and $Cu_B^{2+}$ centers will be discussed in the Results section. In our DNC model, the $C_\alpha$ atoms of Tyr237, His282, His283, Asp372, His376, and His384 are each replaced with a link H atom ($H_{link}$) along the original $C_\beta$-$C_\alpha$ direction with the $C_\beta$-$H_{link}$ distance 1.09 Å. The $C_\gamma$ of

Arg449, N of Gly232, C of His233, and $C_{228}$ of the geranyl sidechain of the $a_3$-heme are also replaced with an $H_{link}$ atom. During geometry optimization calculations, $H_{link}$ atoms on Tyr237, His282, His283, Asp372, His376, His384, and Arg449, and the $C_\alpha$ atom of Gly232 are fixed.

Two DFT exchange-correlation functionals, PW91[44] and OLYP[43,44] with Grimme's dispersion corrections (D3)[47] are used and compared in the current calculations. Fee *et al*. calculated the reaction free energies of several small-molecule reactions which involve oxygen chemistry (e.g. $O_{2gas} + H_{2gas} \rightarrow H_2O_{2gas}$, see Table 3 of Ref 17), and found that in most of the cases, the PW91 potential yields better reaction free energies (closer to experimental results) than B3LYP and B3LYP* DFT hybrid potentials.[17] For the reaction $O_2$(aq) + $4e^-$(from cyt *c*) + $8H^+$(aq,pH=7) → $2H_2O$(liquid) + $4H^+$(aq,pH=3), PW91 also yields the closest reaction free energy (–27.3 kcal $mol^{-1}$) to experiment (–36.9 kcal $mol^{-1}$), compared with the corresponding results obtained from other potentials: OLYP(–19.2 kcal $mol^{-1}$), OPBE(–21.4 kcal $mol^{-1}$), B3LYP(–26.2 kcal $mol^{-1}$), and B3LYP*(–24.7 kcal $mol^{-1}$).[40] On the other hand, based on the calculations for relative spin-state energetics of $Fe^{2+}$ and $Fe^{3+}$ heme models performed by Vancoillie, *et al*,[51] none of the tested density functionals (B3LYP, B3LYP*, OLYP, BP86, TPSS, TPSSh, M06, and M06-L) consistently provides better accuracy than CASPT2 (multiconfigurational perturbation theory) for all their model complexes against available high-level coupled cluster singles and doubles (CCSD) results. However, the pure functional OLYP yields similar results to the hybrid functionals B3LYP* or B3LYP. And for their large heme models, the results of OLYP, B3LYP and B3LYP* are reasonably close to the best estimate of the spin-splittings, with errors typically ≤ 6 kcal $mol^{-1}$.[51] Radoń and Pierloot also investigated the performance of the CASSCF/CASPT2 approach and several DFT functionals (PBE0, B3LYP, BP86, and OLYP) in calculating the bonding of CO, NO, and $O_2$ molecules to two model heme systems.[52] They have found that the experimentally available

binding energies are best reproduced by the CASPT2 method and with the OLYP functional. The CASSCF spin populations most closely correspond to the results obtained with the pure OLYP or BP86 rather than with the hybrid functionals.[52] Therefore, we have used the OLYP functional in studying the geometric, energetic, and Mössbauer properties of *Tt ba*$_3$ C*c*O,[40,50,53] and will also use this functional in the current study.

All calculations are performed using the Amsterdam Density Functional Package (ADF2012.01)[54-56] with integration grid accuracy parameter 4.0 within the conductor like screening (COSMO) solvation model.[57-60] Since both the cluster and the surrounding protein environment are quite polar and contain many water molecules, to be consistent with Refs. 17, [50], and [53], a large dielectric constant of a simple ketone ($\varepsilon$ = 18.5) is applied to the environment in all COSMO calculations. The van der Waals radii 1.5, 1.4, 1.7, 1.52, 1.55, and 1.2 Å are used for atoms Fe, Cu, C, O, N, and H, respectively.[17,50] The triple-$\zeta$ plus polarization (TZP) Slater-type basis set is applied to the Fe and Cu atoms and double-$\zeta$ plus polarization (DZP) basis set to other atoms. The inner cores of C(1s), N(1s), O(1s), Fe(1s,2s,2p), and Cu(1s,2s,2p) are treated by frozen core approximation.

For state [$Fe_{a3}^{3+}$-$(HO_2)^-$-$Cu_B^{2+}$, Tyr237$^-$], we use the "broken-symmetry" (BS) state,[61-63] in which the $Fe_{a3}^{3+}$ site has spin-up electrons as majority spin and the $Cu_B^{2+}$ site has majority spin-down electrons, to represent the low-spin (LS) $Fe_{a3}^{3+}$ site antiferromagnetically (AF) coupling with the $Cu_B^{2+}$ site. Similarly, for state [$Fe_{a3}^{4+}$=$O^{2-}$, $OH^-$-$Cu_B^{2+}$, Tyr237$^\bullet$], we also use BS state calculations to treat the intermediate spin (IS) $Fe_{a3}^{4+}$ site AF-coupling with both $Cu_B^{2+}$ and Tyr237$^\bullet$.

p$K_a$ calculations are also performed in this paper using the following equation[40,50,53] to determine whether the system favors an "extra" proton, and whether the "extra" proton favors residing on His376 or Prop-A:

$$1.37\mathrm{p}K_a = E(\mathrm{A}^-) - E(\mathrm{AH}) + E(\mathrm{H}^+) + \Delta G_{sol}(\mathrm{H}^+,1\mathrm{atm}) - T\Delta S_{gas}(\mathrm{H}^+) + \Delta\mathrm{ZPE} + (5/2)RT \qquad (1)$$

where $E(\mathrm{A}^-)$ and $E(\mathrm{AH})$ are the calculated "total" energies of the deprotonated ($\mathrm{A}^-$) and protonated (AH) states. In ADF, the "total energy" of the system is defined relative to a sum of atomic fragments (spherical spin-restricted atoms). The calculated gas-phase energy of a proton $E(\mathrm{H}^+)$ is therefore relative to a spin-restricted hydrogen atom. $\Delta G_{sol}(\mathrm{H}^+,1\mathrm{atm})$ is the solvation free energy of a proton at 1 atm pressure. We use the "best available" experimental value of –264.0 kcal $\mathrm{mol}^{-1}$ for this term, based on analysis of cluster-ion solvation data.[64-67] For $E(\mathrm{H}^+)$, here we take the empirically corrected values 291.5 kcal $\mathrm{mol}^{-1}$ (i.e. 12.64 eV) for PW91 and 293.1 kcal $\mathrm{mol}^{-1}$ (i.e. 12.71 eV) for OLYP based on experimental standard hydrogen electrode energy and the proton solvation free energy (see Appendix in Ref. 40). The translational entropy contribution to the gas-phase free energy of a proton is taken as $-T\Delta S_{gas}(\mathrm{H}^+) = -7.8$ kcal $\mathrm{mol}^{-1}$ at 298 K and 1 atm pressure.[68] $(5/2)RT = 1.5$ kcal $\mathrm{mol}^{-1}$ includes the proton translational energy $(3/2)RT$ and $PV = RT$.[68] The term ΔZPE is the zero point energy difference for the deprotonated state ($\mathrm{A}^-$) minus the protonated state (AH), and it is usually about –8.0 kcal $\mathrm{mol}^{-1}$. For simplicity we take ΔZPE = –8.0 kcal $\mathrm{mol}^{-1}$ in this paper for both PW91 and OLYP calculations on His376 and Prop-A.[53]

## Results and Discussion

### Hydroperoxo DNC State [$Fe_{a3}^{3+}$-$(O\text{-}OH)^-$-$Cu_B^{2+}$, $Tyr237^-$] *vs.* [$Fe_{a3}^{3+}$-$(HO\text{-}O)^-$-$Cu_B^{2+}$, $Tyr237^-$] with Neutral His376 or Protonated $His376^+$

Depending on which oxygen atom (O1 or O2, see Figure 1) becomes protonated, potentially there are two forms of the hydroperoxo DNC state: (**1**) [$Fe_{a3}^{3+}$-$(O\text{-}OH)^-$-$Cu_B^{2+}$, $Tyr237^-$], where the proton is on O2 that is closer to $Cu_B$; and (**2**) [$Fe_{a3}^{3+}$-$(HO\text{-}O)^-$-$Cu_B^{2+}$, $Tyr237^-$], where the proton is on O1 that is closer to $Fe_{a3}$. Form (**1**) is ready for the O-O bond cleavage. It is likely that the proton

from Tyr237 directly transfers (through one or two water molecules) to atom O2.[39] However, if the bridging peroxo [$Fe_{a3}^{3+}$-(O1-O2)$^{2-}$-$Cu_B^{2+}$, Tyr237] state is really formed before the proton transfer,[17,33,34,39,40] the atom O1 is actually closer to the –OH group of Tyr237. Here by energetic comparisons, we will see whether the proton favors residing on O1 or O2.

The central DNC structures of the [$Fe_{a3}^{3+}$-(O-OH)$^-$-$Cu_B^{2+}$, Tyr237$^-$] and [$Fe_{a3}^{3+}$-(HO-O)$^-$-$Cu_B^{2+}$, Tyr237$^-$] states are given in Figure 3A and 3B, respectively. Two water molecules HOH604 and HOH608 were observed above the dioxygen species in the DNC of the radiolyticly reduced X-ray crystal structure 3S8G.[15] HOH608 is within H-bonding distance with both the carbonyl of Gly232 and HOH604.[15] We also kept these two water molecules in our DNC models. In [$Fe_{a3}^{3+}$-(O-OH)$^-$-$Cu_B^{2+}$, Tyr237$^-$], the proton on O2 has H-bonding interaction with HOH608 (Figure 3A). While in [$Fe_{a3}^{3+}$-(HO-O)$^-$-$Cu_B^{2+}$, Tyr237$^-$], HOH608 H-bonds with O2 (Figure 3B).

We will use $Fe^{3+}$-(O-OH)$^-$-$Cu^{2+}$-Y237$^-$-H376/H376$^+$ and $Fe^{3+}$-(HO-O)$^-$-$Cu^{2+}$-Y237$^-$-H376/H376$^+$ (204/205 atoms in the model) to represent the [$Fe_{a3}^{3+}$-(O-OH)$^-$-$Cu_B^{2+}$, Tyr237$^-$] and [$Fe_{a3}^{3+}$-(HO-O)$^-$-$Cu_B^{2+}$, Tyr237$^-$] states with neutral-His376/protonated-His376$^+$, respectively. The geometries of the four DNC clusters have been optimized with both PW91 and OLYP potentials with Grimme's dispersion corrections (D3).[47] The main geometric, energetic, p$K_a$(His376), and Mulliken net spin population properties of the eight optimized DNC models are given in Table 1.

The "extra" proton on His376 has no significant effect on the DNC structures of both $Fe^{3+}$-(O-OH)$^-$-$Cu^{2+}$-Y237$^-$ and $Fe^{3+}$-(HO-O)$^-$-$Cu^{2+}$-Y237$^-$ states. However, both states favor having the extra proton on His376 with the calculated p$K_a$(H376) value in the range 11.0-11.7 for the PW91-D3 and OLYP-D3 calculations.

The PW91-D3 and OLYP-D3 calculated energies of the $Fe^{3+}$-(HO-O)$^-$-$Cu^{2+}$-Y237$^-$-H376/H376$^+$ states are more than 10 kcal mol$^{-1}$ higher than the corresponding energies of the $Fe^{3+}$-

$(O\text{-}OH)^{-}$-$Cu^{2+}$-Y237$^{-}$-H376/H376$^{+}$ states, showing that the proton transferred from Tyr237 would reside on atom O2 rather than O1, and the O-O bond is ready to cleave after O2 receives the proton.

The calculated net spins (0.81/0.89) on the $Fe_{a3}$ site in $Fe^{3+}$-$(O\text{-}OH)^{-}$-$Cu^{2+}$-Y237$^{-}$-H376$^{+}$ obtained from PW91-D3/OLYP-D3 calculations reflect that the $Fe_{a3}$ is in low-spin $Fe_{a3}^{3+}$ state. The negative sign of the net spins on the $Cu_B$ site (–0.37/–0.30) show that the spins of the $Fe_{a3}$ and $Cu_B$ sites are AF-coupled. The net spin values on $Cu_B$, especially in OLYP-D3 calculations (–0.30), are rather small for a $Cu_B^{2+}$ site. On the other hand, the Tyr237$^{-}$ ring shows substantial net spins with overall –0.34 in PW91-D3 and –0.52 in OLYP-D3 calculations (about 1/3 the net spins are on the O atom). Therefore, the $Cu_B$ and Tyr237 are in the mixed state between $Cu_B^{2+}$-Tyr237$^{-}$ and $Cu_B^{+}$-Tyr237$^{\bullet}$. In OLYP-D3 calculations, the $Cu_B$ has more $Cu_B^{+}$ character, which results in a little longer Cu-O2 and shorter O1-O2 distances in $Fe^{3+}$-$(O\text{-}OH)^{-}$-$Cu^{2+}$-Y237$^{-}$-H376$^{+}$ than for the corresponding PW91-D3 optimized structure.

**The $P_M$ DNC State [$Fe_{a3}^{4+}$=$O^{2-}$…$OH^{-}$-$Cu_B^{2+}$, Tyr237$^{\bullet}$] *vs.* [$Fe_{a3}^{4+}$=$O^{2-}$···$HO^{-}$-$Cu_B^{2+}$, Tyr237$^{\bullet}$] with Neutral His376 or Protonated His376$^{+}$**

After the cleavage of the O-O bond from the $Fe^{3+}$-$(O\text{-}OH)^{-}$-$Cu^{2+}$-Y237$^{-}$-H376$^{+}$ state, both $Fe_{a3}^{3+}$ and Tyr237$^{-}$ donate an electron to the hydroperoxo group ($O_2H^{-}$) and become $Fe_{a3}^{4+}$ and Tyr237$^{\bullet}$ radical, respectively. There are also two potential DNC structures of the $\mathbf{P_M}$ state can be formed: (**1**) [$Fe_{a3}^{4+}$=$O^{2-}$…$OH^{-}$-$Cu_B^{2+}$, Tyr237$^{\bullet}$] (see Figure 4A for the central portion of this DNC cluster). In this state, which is formed by increasing of the O1-O2 distance, the newly formed $OH^{-}$ group that binds with $Cu_B$ may keep the H-bonding interaction with HOH608. (**2**) [$Fe_{a3}^{4+}$=$O^{2-}$···$HO^{-}$-$Cu_B^{2+}$, Tyr237$^{\bullet}$]. As shown in Figure 4B, during the O1-O2 cleavage, the proton on O2 may rotate toward O1 and form a H-bonding interaction with O1. Meanwhile the proton on

HOH608 which has no interaction with other groups can rotate toward O2 and form a H-bonding interaction with O2. In order to see which form of the two $\mathbf{P_M}$ models is energetically more favorable, and whether it is energetically favorably for His376 to remain protonated His376$^+$, we have geometry optimized these two forms of the $\mathbf{P_M}$ models in both neutral His376 and cationic His376$^+$ states with both PW91-D3 and OLYP-D3 potentials.

Similar to the section above, here we use $Fe^{4+}=O^{2-}\cdots OH^{-}$-$Cu^{2+}$-Y237$^{\bullet}$-H376/H376$^+$ and $Fe^{4+}=O^{2-}\cdots HO^{-}$-$Cu^{2+}$-Y237$^{\bullet}$-H376/H376$^+$ to represent the [$Fe_{a3}^{4+}=O^{2-}\cdots OH^{-}$-$Cu_B^{2+}$, Tyr237$^{\bullet}$] and [$Fe_{a3}^{4+}=O^{2-}\cdots HO^{-}$-$Cu_B^{2+}$, Tyr237$^{\bullet}$] states with neutral-His376/protonated-His376$^+$, respectively. The main calculated properties of these DNC clusters are given in Table 2.

After the cleavage of the O-O bond, the net spin values on $Cu_B$ (0.48-0.52) and Tyr237 (0.71-0.93), especially in the geometry optimized $Fe^{4+}=O^{2-}\cdots HO^{-}$-$Cu^{2+}$-Y237$^{\bullet}$-H376/H376$^+$ states are significantly increased in both PW91-D3 and OLYP-D3 calculations, showing $Cu_B$ and Tyr237 are indeed in the $Cu_B^{2+}$ and Tyr237$^{\bullet}$ radical states. In the ideal ionic limit, the net unpaired spin population for an intermediate-spin $Fe^{4+}$ site is 2 (the Mulliken unpaired spin population is measured in unpaired electron spin units, so 2 unpaired spins corresponds to total spin $S$ = 1). However, the absolute calculated net-spins on $Fe_{a3}^{4+}$ in Table 2 are all smaller than 2. In fact, the sum of the net-spins on $Fe_{a3}^{4+}$ (1.11-1.25) and O1 (0.75-0.88) for each DNC cluster is about 2, indicative of substantial $Fe_{a3}^{4+}=O^{2-}$ covalency.

PW91-D3 and OLYP-D3 calculations yield very similar results for Fe-O1 and Cu-O2 distances in Table 2. However, the O1-O2 distances predicted by the PW91-D3 potential, especially for the $Fe^{4+}=O^{2-}\cdots OH^{-}$-$Cu^{2+}$-Y237$^{\bullet}$-H376/H376$^+$ clusters, are much shorter (by 0.23-0.39 Å) than the corresponding values predicted by the OLYP-D3 potential. At this shorter distance, one expects increased repulsion between the oxygen atoms O1 and O2 for PW91-D3 compared to OLYP-D3 in

the $Fe^{4+}=O^{2-}\ldots OH^{-}$-$Cu^{2+}$-Y237$^{\bullet}$-H376/H376$^{+}$ cluster, consistent with the trend in the reaction energy for O-O bond cleavage. Starting from $Fe^{3+}$-$(O\text{-}OH)^{-}$-$Cu^{2+}$-Y237$^{-}$-H376/H376$^{+}$, the reaction energy is only 2.3/3.9 kcal mol$^{-1}$ in PW91-D3, compared to 10.9/12.0 kcal mol$^{-1}$ in OLYP-D3 calculations. However, both for PW91-D3 and OLYP-D3, the energies of the $Fe^{4+}=O^{2-}\cdots HO^{-}$-$Cu^{2+}$-Y237$^{\bullet}$-H376/H376$^{+}$ states are much lower than the corresponding $Fe^{4+}=O^{2-}\ldots OH^{-}$-$Cu^{2+}$-Y237$^{\bullet}$-H376/H376$^{+}$ states (by 6.9-14.7 kcal mol$^{-1}$). These results indicate the presence of strong hydrogen bonding across the $Fe^{4+}=O^{2-}\cdots HO^{-}$-$Cu^{2+}$ bridge. Further, the p$K_a$ calculations show that the His376 side chain is still in the protonated His376$^{+}$ form. Therefore, after O-O cleavage, the $\mathbf{P_M}$ state of the DNC favors the $Fe^{4+}=O^{2-}\cdots HO^{-}$-$Cu^{2+}$-Y237$^{\bullet}$-H376$^{+}$ conformation with H-bonding between $Fe^{4+}=O^{2-}$ and $HO^{-}$-$Cu^{2+}$ and with an "extra" proton on His376$^{+}$.

**Energy Barriers of the O-O Cleavage in $Fe^{3+}$-$(O\text{-}OH)^{-}$-$Cu^{2+}$-Y237$^{-}$-H376/H376$^{+}$ → $Fe^{4+}=O^{2-}\cdots HO^{-}$-$Cu^{2+}$-Y237$^{\bullet}$-H376/H376$^{+}$**

In the above sections, we have concluded that the hydroperoxo state of the DNC favors the $Fe^{3+}$-$(O\text{-}OH)^{-}$-$Cu^{2+}$-Y237$^{-}$-H376$^{+}$ conformation (Figure 3A) with the proton on O2 and with an "extra" proton on His376$^{+}$. If the O1-O2 bond is cleaved, this DNC structure will transit to the $Fe^{4+}=O^{2-}\cdots HO^{-}$-$Cu^{2+}$-Y237$^{\bullet}$-H376$^{+}$ state (Figure 4B). In order to estimate the energy barrier of the O1-O2 cleavage, a path that connects the $Fe^{3+}$-$(O\text{-}OH)^{-}$-$Cu^{2+}$-Y237$^{-}$-H376$^{+}$ and $Fe^{4+}=O^{2-}\cdots HO^{-}$-$Cu^{2+}$-Y237$^{\bullet}$-H376$^{+}$ optimized geometries is constructed individually for PW91-D3 and OLYP-D3 potentials by linear interpolation of the Cartesian-coordinates. Then constrained geometry optimization calculations were performed on these transit structures by fixing the O1 and O2 positions (and the $H_{link}$ atoms). For the structures with O1-O2 distance in the region (1.65 Å, 1.90 Å), both H-bonding patterns shown in Figure 4A and 4B were geometry optimized, in order to get

the lower-energy conformation. To see if the extra proton on His376$^+$ affects this transition barrier, we also performed similar PW91-D3/OLYP-D3 constrained geometry optimizations on the $Fe^{3+}$-$(O\text{-}OH)^-$-$Cu^{2+}$-$Y237^-$-H376 → $Fe^{4+}$=$O^{2-}$···$HO^-$-$Cu^{2+}$-$Y237^{\bullet}$-H376 path. Then for each optimized structure along this path, the relative energy ($\Delta E$) to the corresponding PW91-D3/OLYP-D3 geometry optimized $Fe^{3+}$-$(O\text{-}OH)^-$-$Cu^{2+}$-$Y237^-$-H376/H376$^+$ state was calculated. The relative energy plots *vs*. the O1-O2 distance for the four $Fe^{3+}$-$(O\text{-}OH)^-$-$Cu^{2+}$-$Y237^-$-H376/H376$^+$ → $Fe^{4+}$=$O^{2-}$···$HO^-$-$Cu^{2+}$-$Y237^{\bullet}$-H376/H376$^+$ transitions obtained from PW91-D3 and OLYP-D3 calculations are shown in Figure 5.

Surprisingly, the barriers of these four reaction paths are all very small. When His376 is in neutral state, the highest energy obtained for the $Fe^{3+}$-$(O\text{-}OH)^-$-$Cu^{2+}$-$Y237^-$-H376 → $Fe^{4+}$=$O^{2-}$···$HO^-$-$Cu^{2+}$-$Y237^{\bullet}$-H376 transition is 2.4 kcal mol$^{-1}$ for PW91-D3 and 1.6 kcal mol$^{-1}$ for OLYP-D3. When an extra proton is on His376, the highest-energy barely changes to 2.6 and 0.9 kcal mol$^{-1}$, in PW91-D3 and OLYP-D3 calculations, respectively. Therefore, the extra proton on His376 does not have a significant effect on the O-O bond cleavage barrier. In Ref 40 (state **$6_2$** → **6**), we have computed the energy cost from neutral Tyr237 to the ferric peroxo isomer [$Fe_{a3}^{3+}$-$(O\text{-}O)^{2-}$-$Cu_B^{2+}$, Tyr237], which is 6 kcal mol$^{-1}$ in PW91-D3 and 6.5 kcal mol$^{-1}$ in OLYP-D3 calculations. This additional cost should be added to the cumulative barrier[69] of the **A** → $\mathbf{P_M}$ transition. Then the **A** → $\mathbf{P_M}$ activation energy is around 8.6/7.4 kcal mol$^{-1}$ in PW91-D3/OLYP-D3 calculations. Therefore, the experimental **A** → $\mathbf{P_M}$ barrier of 10.2 kcal mol$^{-1}$ is closely predicted by both PW91-D3 and OLYP-D3 calculations. The rate limiting step of the **A** → $\mathbf{P_M}$ transition is the proton transfer from Tyr237 to O-O. Once the hydroperoxo state $Fe^{3+}$-$(O\text{-}OH)^-$-$Cu^{2+}$-$Y237^-$-H376$^+$ is formed, the O-O bond is readily cleaved.

The calculated properties of the four highest-energy structures of the four profiles in Figure 5 are given in Table 3. The DNC reaches the highest energy when the O1-O2 distance increases by ~0.2 Å from the initial $Fe^{3+}$-$(O\text{-}OH)^{-}$-$Cu^{2+}$-$Y237^{-}$-H376/$H376^{+}$ state. The calculated net spin values on $Fe_{a3}$, $Cu_B$, and Tyr237 in the four structures are all similar to the corresponding values in the $Fe^{3+}$-$(O\text{-}OH)^{-}$-$Cu^{2+}$-$Y237^{-}$-H376/$H376^{+}$ state, as would be expected for an early transition state.

**Testing Protonation of Prop-A at Two Alternative Positions**

Our calculations have shown that, both $Fe^{3+}$-$(O\text{-}OH)^{-}$-$Cu^{2+}$-$Y237^{-}$ and $Fe^{4+}{=}O^{2-}\cdots HO^{-}$-$Cu^{2+}$-$Y237^{\bullet}$ states energetically favor an extra proton on His376. In this section, through p$K_a$ calculations, we will study if this "extra" proton would stay on the carboxylate group of Prop-A instead. Theoretically Prop-A can be protonated either at the oxygen atom (we will call it position 1) which is close to Asp372, or at the oxygen atom (position 2) which H-bonds to HOH609 (see Figure 2). Here we investigate different H-bonding pattern of Prop-A with protonation on position 1 or 2. Site-directed mutagenesis experiments have shown that the proton pumping in $ba_3$ C*c*O from *Tt* is inhibited by the single Asp372Ile mutation.[70] Asp372 therefore plays a critical role in the proton transfer (pumping) pathway. The carboxylate groups of Asp372 and Prop-A are within a strong H-bonding distance in all available X-ray crystal structures of *Tt* $ba_3$ C*c*O.[10-12,15] Therefore Asp372 is usually considered being in the neutral protonated state (Figure 2).[17] In order to add a proton to position 1 of Prop-A in Figure 2, we assume proton transfers from the K-path → Tyr237 → nearby residues (possibly Thr302)[71] and $H_2O$ molecules → HOH583 → Asp372 → PropA. We then modified the proton positions of Asp372 and HOH583 in Figure 2 and obtained a DNC model with protonated Prop-A at position 1 (Prop-A-H.1, see Figure 6). This protonated carboxylate of Prop-A can rotate, or this proton can move from position 1 to 2, we then constructed another DNC model with protonated Prop-A at position 2 (Prop-A-H.2, see Figure 7).

Using both PW91-D3 and OLYP-D3 methods, we have optimized the geometries of the $Fe^{3+}$-(O-OH)$^{-}$-$Cu^{2+}$-Y237$^{-}$-Prop-A-H.1,2 and $Fe^{4+}$=$O^{2-}$···HO$^{-}$-$Cu^{2+}$-Y237$^{\bullet}$-Prop-A-H.1,2 states. The main calculated properties of the four states are given in Table 4.

It is obvious that the system highly disfavors the extra proton on Prop-A. The calculated p$K_a$'s of the Prop-A site (note that the non-protonated Prop-A states are $Fe^{3+}$-(O-OH)$^{-}$-$Cu^{2+}$-Y237$^{-}$-H376 given in Table 1 and $Fe^{4+}$=$O^{2-}$···HO$^{-}$-$Cu^{2+}$-Y237$^{\bullet}$-H376 in Table 2) are even below zero in PW91-D3 calculations (–3.4, –3.9, –2.6, and –2.6) and are near zero in OLYP-D3 results (0.2, 0.3, 0.5, and 1.1). The energies of the four $Fe^{3+}$-(O-OH)$^{-}$-$Cu^{2+}$-Y237$^{-}$-Prop-A-H.1,2/$Fe^{4+}$=$O^{2-}$···HO$^{-}$-$Cu^{2+}$-Y237$^{\bullet}$-Prop-A-H.1,2 states are much higher than the corresponding $Fe^{3+}$-(O-OH)$^{-}$-$Cu^{2+}$-Y237$^{-}$-H376$^{+}$/$Fe^{4+}$=$O^{2-}$···HO$^{-}$-$Cu^{2+}$-Y237$^{\bullet}$-H376$^{+}$ states (in Tables 1 and 2) by 20.0, 20.8, 19.7, and 19.7 kcal mol$^{-1}$ in PW91-D3 and by 14.8, 14.7, 15.4, and 14.6 kcal mol$^{-1}$ in OLYP-D3 calculations, respectively. Therefore, the extra proton would reside on His376, but not on Prop-A. The carboxylate group of Prop-A can be a part of the proton transfer pathway to pass on, but unlikely to hold the proton as a PLS.

## Conclusions

Our current broken-symmetry DFT calculations on the DNC models of *ba*$_3$ C*c*O from *Tt* show that, if the bridging [$Fe_{a3}^{3+}$-(O1-O2)$^{2-}$-$Cu_B^{2+}$, Tyr237] state exists, atom O2, which is farther from $Fe_{a3}$, should receive the $H^+$ (originated from Tyr237) to form the hydroperoxo [$Fe_{a3}^{3+}$-(O-OH)$^{-}$-$Cu_B^{2+}$, Tyr237$^{-}$] state before the O-O bond cleavage. The calculated net spin values indicate that, $Cu_B$ and Tyr237 appear as a mixture of $Cu_B^{2+}$-Tyr237$^{-}$ and $Cu_B^{+}$-Tyr237$^{\bullet}$ in the [$Fe_{a3}^{3+}$-(O-OH)$^{-}$-$Cu_B^{2+}$, Tyr237$^{-}$] state, and this $Cu_B$ site has more $Cu_B^{+}$ character in OLYP-D3 than in PW91-D3 calculations.

After the O-O bond cleavage, the $\mathbf{P_M}$ state with Tyr237$^{\bullet}$ radical has the DNC conformation of [$Fe_{a3}^{4+}$=$O^{2-}$···$HO^{-}$-$Cu_B^{2+}$, Tyr237$^{\bullet}$] with inner H-bonding interaction between $O^{2-}$ and $HO^{-}$. The calculated O-O bond cleavage barrier in the transition of [$Fe_{a3}^{3+}$-$(O\text{-}OH)^{-}$-$Cu_B^{2+}$, Tyr237$^{-}$] → [$Fe_{a3}^{4+}$=$O^{2-}$···$HO^{-}$-$Cu_B^{2+}$, Tyr237$^{\bullet}$] is very small in both PW91-D3 and OLYP-D3 calculations (0.9-2.6 kcal mol$^{-1}$). Therefore, the rate limiting step of the **A** → $\mathbf{P_M}$ transition is the proton transfer from Tyr237 to $O_2$.

Our calculations on the [$Fe_{a3}^{3+}$-$(O\text{-}OH)^{-}$-$Cu_B^{2+}$, Tyr237$^{-}$] and [$Fe_{a3}^{4+}$=$O^{2-}$···$HO^{-}$-$Cu_B^{2+}$, Tyr237$^{\bullet}$] DNC's also show that, the system highly favors an extra proton on His376 in these states, but not on the carboxylate group of Prop-A. A histidine residue at the position of His376 is totally conserved in all B-type C*c*O's.[71] Based on the site-directed mutagenesis experiments on *ba*$_3$ C*c*O from *Tt*,[70,71] Asp372, Prop-A, His376, and the nearby water molecules play an important role for proton pumping. The mutants His376Asn and Asp372Ile fail to pump protons.[70,71] Our recent molecular dynamics simulations (manuscript under preparation) show that the imidazole group of His376 can easily rotate. This function is important for His376 to uptake the extra proton and serve as the proton loading site. We propose that when the system favors an extra proton on His376, the concerted proton transfer starting from the K-path will occur, in which Asp372 donates its proton to Prop-A and meanwhile receives a proton originated from the K-path, and the imidazole ring of His376 rotates to get the proton from Prop-A and becomes His376$^{+}$. Because the system is strongly against an extra proton on Prop-A (when Asp372 is neutral-protonated), His376$^{+}$ cannot give back the extra proton to Prop-A. Therefore, the pair of Prop-A/neutral-Asp372 serves as the gate to prevent the proton from back-flowing to the DNC. The X-ray crystal structures show that the carboxylate group of Glu126$^{II}$ (in subunit II) is close to the $N_{\varepsilon 2}$ atom (on top of Figure 2) of His376.[10-12,15] When the extra proton on His376 needs to be pumped out at a certain state of the

catalytic cycle, the carboxylate of $Glu126^{II}$ can pick up this proton and rotate about its $C_\beta$-$C_\gamma$ and $C_\gamma$-$C_\delta$ bonds to swing into the outside region where there are charged side chains and numerous water molecules.[17] However, this $Glu126^{II}$ is not essential for proton pumping, since it can be mutated without loss of function.[71] Therefore, the extra proton on $His376^+$ can also be picked up by other residues or water molecules and transferred out of the enzyme.

## Supporting Information

The Cartesian coordinates for the optimized clusters discussed in Tables 1-4 with protonated prop-A or $His376^+$ are given as supporting information.

## Acknowledgment

It is a great pleasure to dedicate this article to Prof. Evert Jan Baerends in honor of his 70th birthday. One of us (LN) worked with Evert Jan as a postdoc at VU Amsterdam about 35 years ago, while another (AWG) worked with him 30 years later. We thank NIH for financial support (R01 GM100934). L. Yang appreciates the support and help from Professor Sanguo Hong, Ning Zhang, and Hongming Wang from Nanchang University, China, and the funding from China Scholarship Council (CSC) for a two-year research visit in the USA. We also thank the computational resources from The Scripps Research Institute. This work also used the Extreme Science and Engineering Discovery Environment (XSEDE), which is supported by National Science Foundation (grant number ACI-1053575, resources at the San Diego Supercomputer Center through award TG-CHE130010 to AWG).

# Caption of Figures

**Figure 1.** The $Fe_{a3}$ and $Cu_B$ dinuclear center (DNC) observed in the radiolyticly reduced X-ray crystal structure (pdb code: 3S8G with 1.7 Å resolution)[15] of $ba_3$ C*c*O from *Thermus thermophilus* (*Tt*). This figure is revised with permission from Figure 1 of Ref [50]. Copyright 2013, American Chemical Society.

**Figure 2.** The water molecules and the H-bonding residue sidechains above the DNC in the X-ray crystal structure 3S8G.[15] Note that in $His376^+$ state, an extra proton is added on top ($N_{\varepsilon 2}$) of His376 side chain. This figure is revised with permission from Figure 2 of Ref [50]. Copyright 2013, American Chemical Society.

**Figure 3.** The central portions of the hydroperoxo DNC models. **A**: [$Fe_{a3}^{3+}$-$(O\text{-}OH)^-$-$Cu_B^{2+}$, $Tyr237^-$] with H on O2. **B**: [$Fe_{a3}^{3+}$-$(HO\text{-}O)^-$-$Cu_B^{2+}$, $Tyr237^-$] with H on O1.

**Figure 4.** The central portions of two feasible DNC models for the $\mathbf{P_M}$ state after the O-O bond cleavage. **A**: [$Fe_{a3}^{4+}$=$O^{2-}$…$OH^-$-$Cu_B^{2+}$, $Tyr237^\bullet$] in which the $OH^-$ group H-bonds with HOH608. **B**: [$Fe_{a3}^{4+}$=$O^{2-}$···$HO^-$-$Cu_B^{2+}$, $Tyr237^\bullet$] in which the $OH^-$ group H-bonds with $O^{2-}$ (O1).

**Figure 5.** PW91-D3 and OLYP-D3 transitional energy plots *vs*. O1-O2 distances along the $Fe^{3+}$-$(O\text{-}OH)^-$-$Cu^{2+}$-$Y237^-$-H376/$H376^+$ → $Fe^{4+}$=$O^{2-}$···$HO^-$-$Cu^{2+}$-$Y237^\bullet$-H376/$H376^+$ (Fig. 3A → Fig. 4B) pathway. Energies are relative to the corresponding geometry optimized $Fe^{3+}$-$(O\text{-}OH)^-$-$Cu^{2+}$-$Y237^-$-H376/$H376^+$ state. 1) Blue circles: OLYP-D3 calculations with neutral His376. 2) Red squares: OLYP-D3 calculations with protonated $His376^+$. 3) Green diamonds: PW91-D3 calculations with neutral His376. 4) Purple triangles: PW91-D3 calculations with protonated $His376^+$. The calculated properties of the highest-energy structures are given in Table 3.

**Figure 6.** An extra proton is added to Prop-A at position 1.

**Figure 7.** An extra proton is added to Prop-A at position 2.

**Figure 1.**

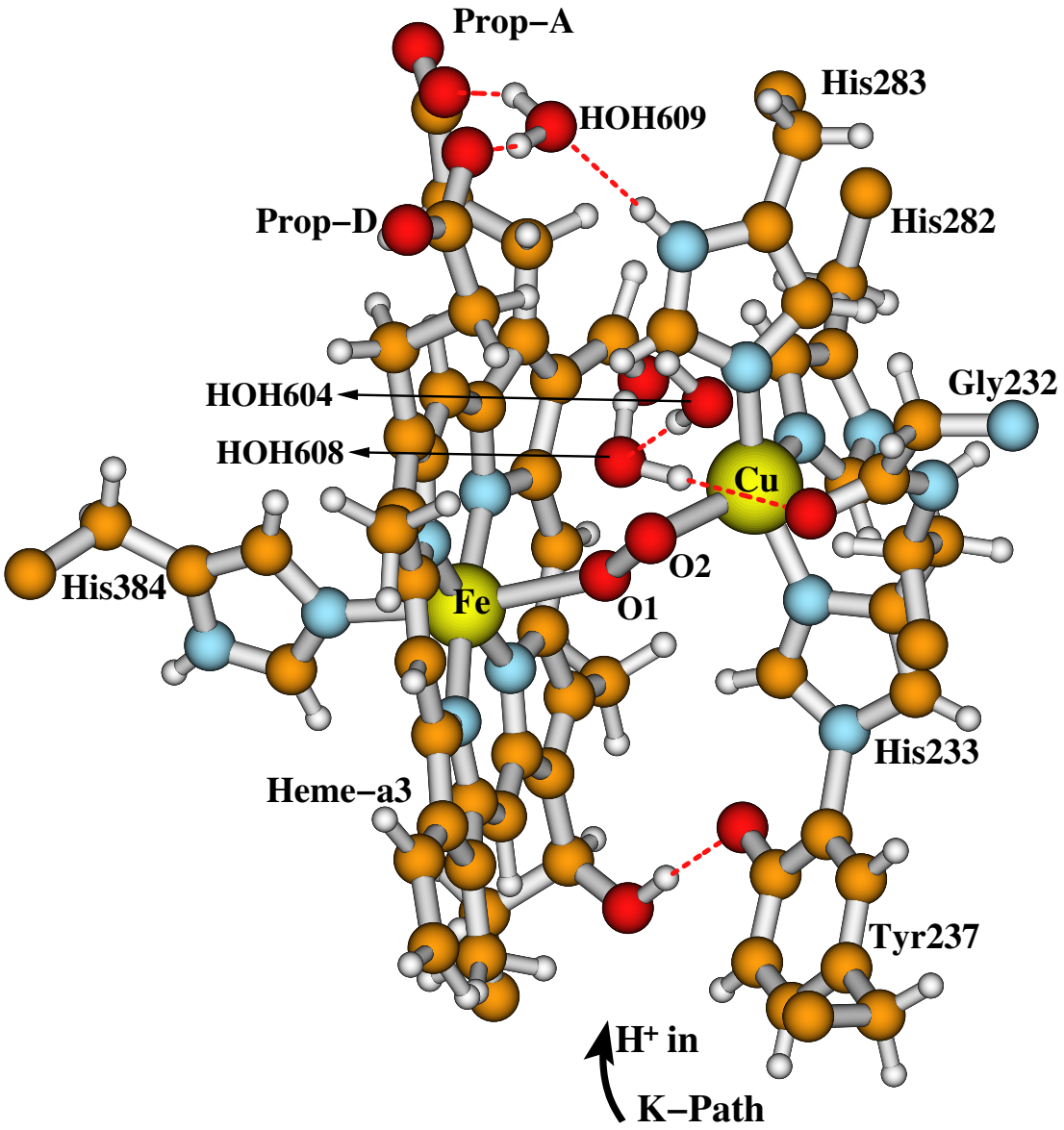

**Figure 2.**

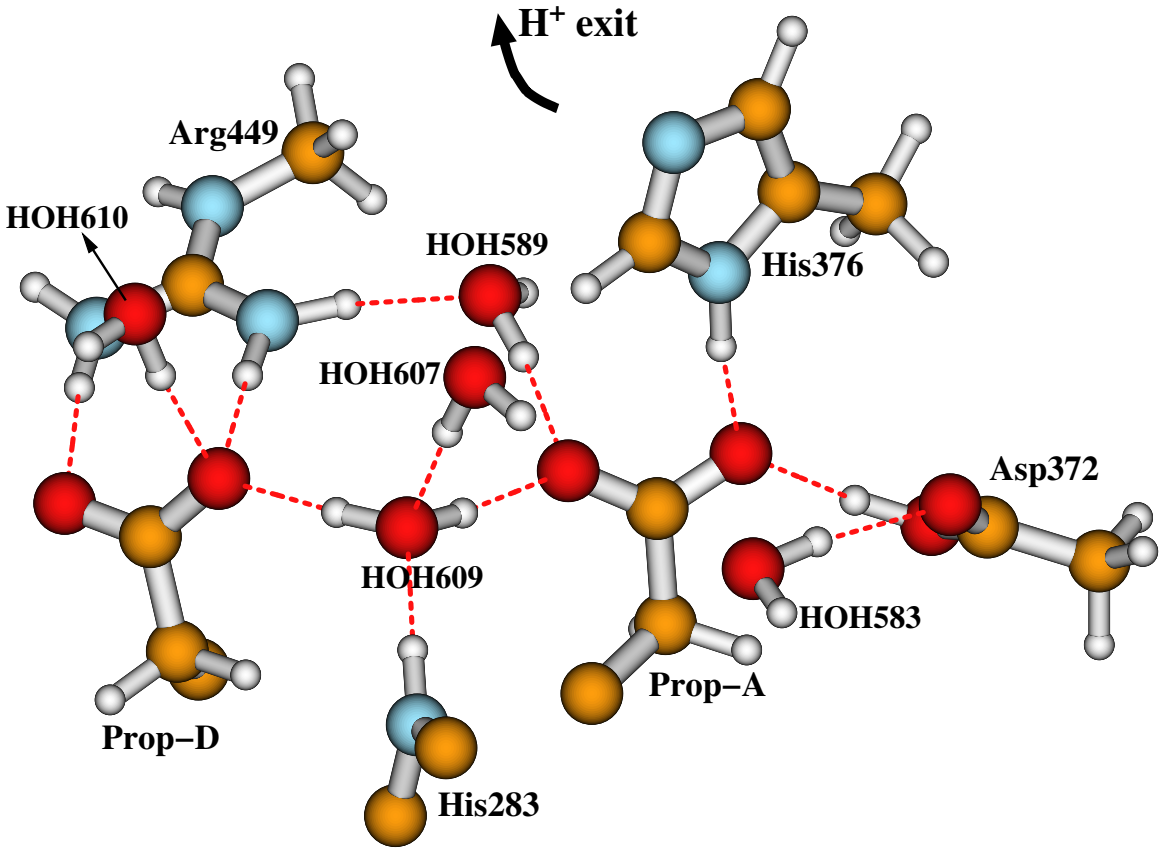

**Figure 3.**

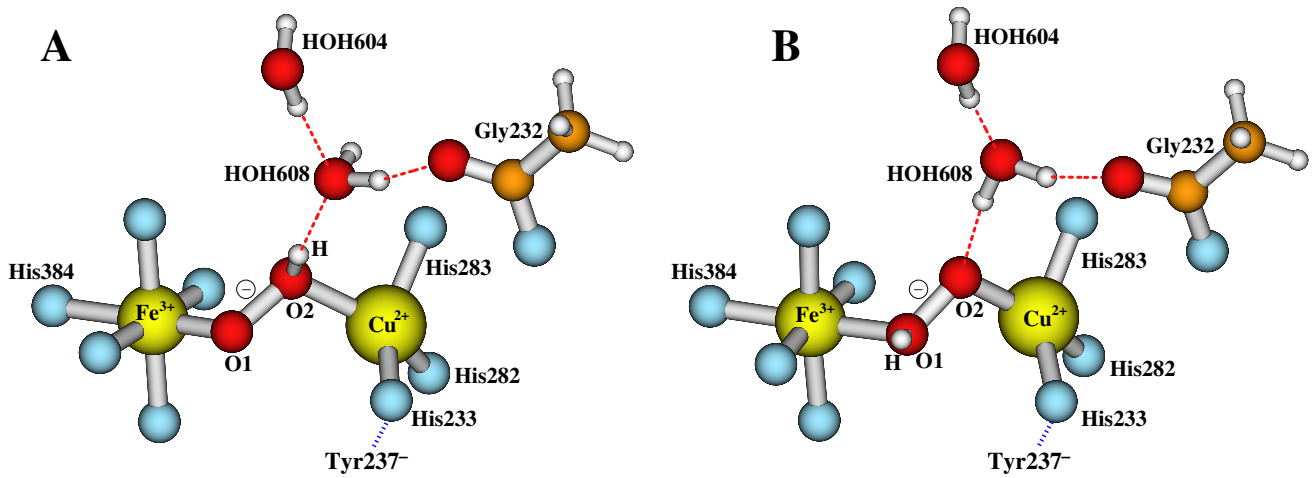

**Figure 4.**

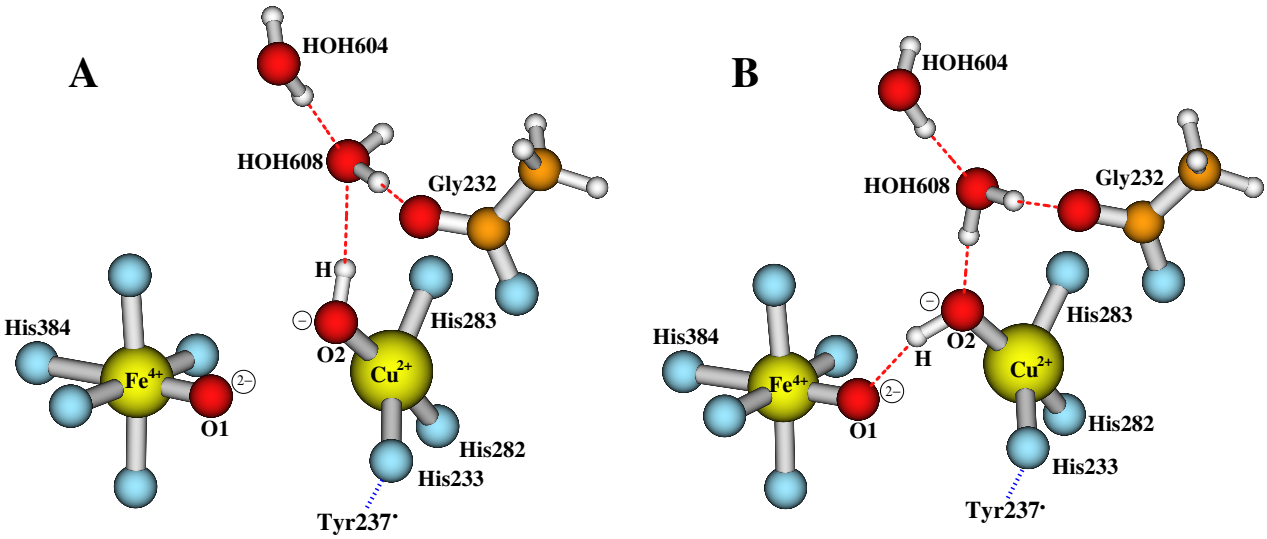

**Figure 5**.

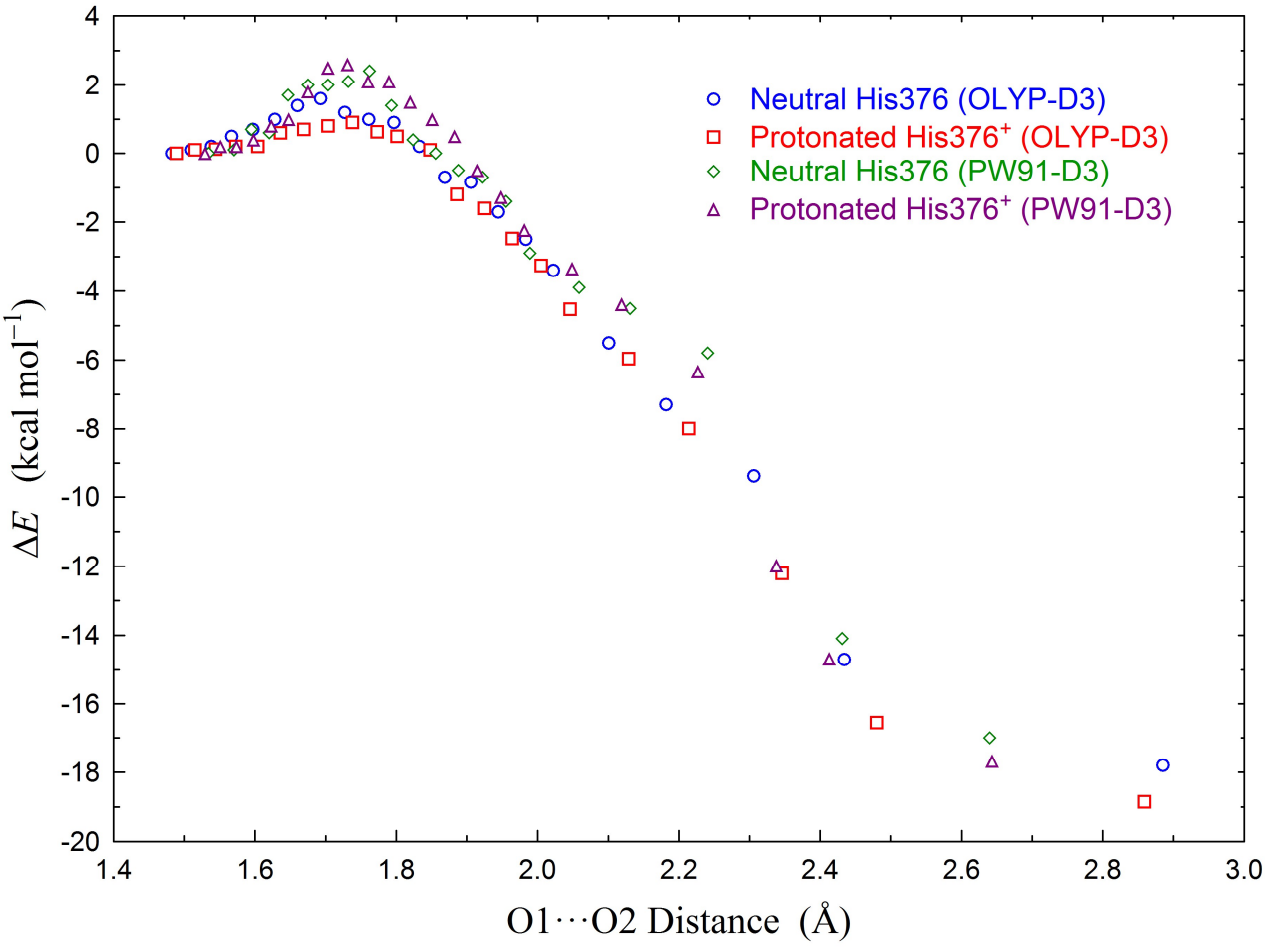

**Figure 6**.

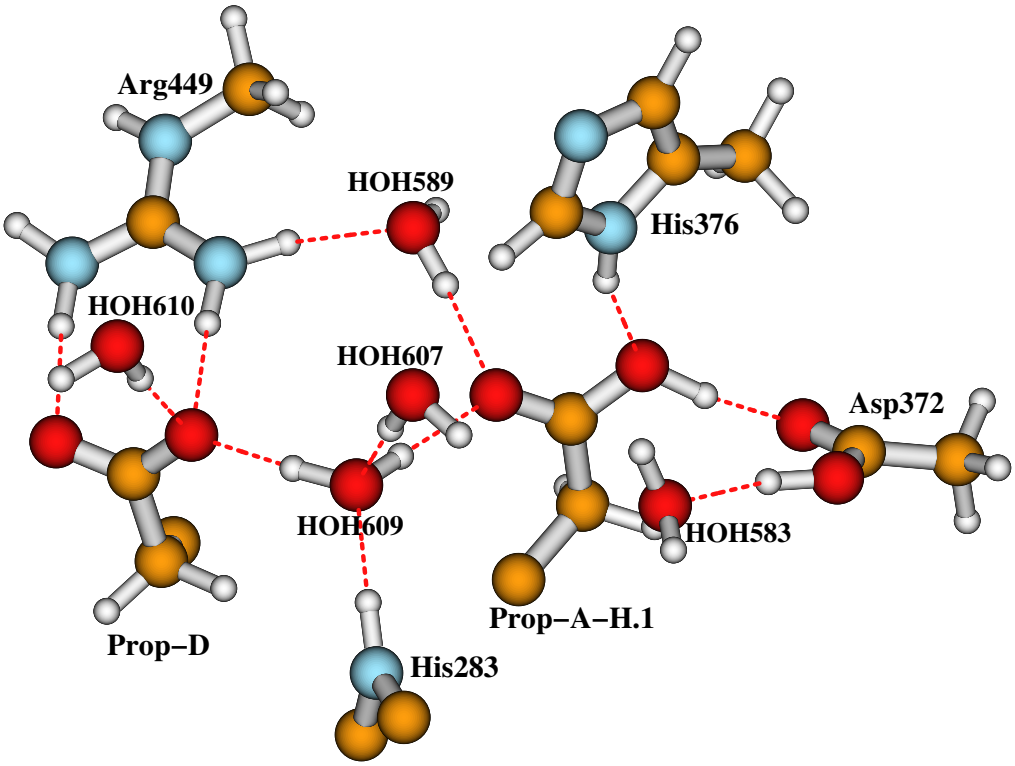

**Figure 7**.

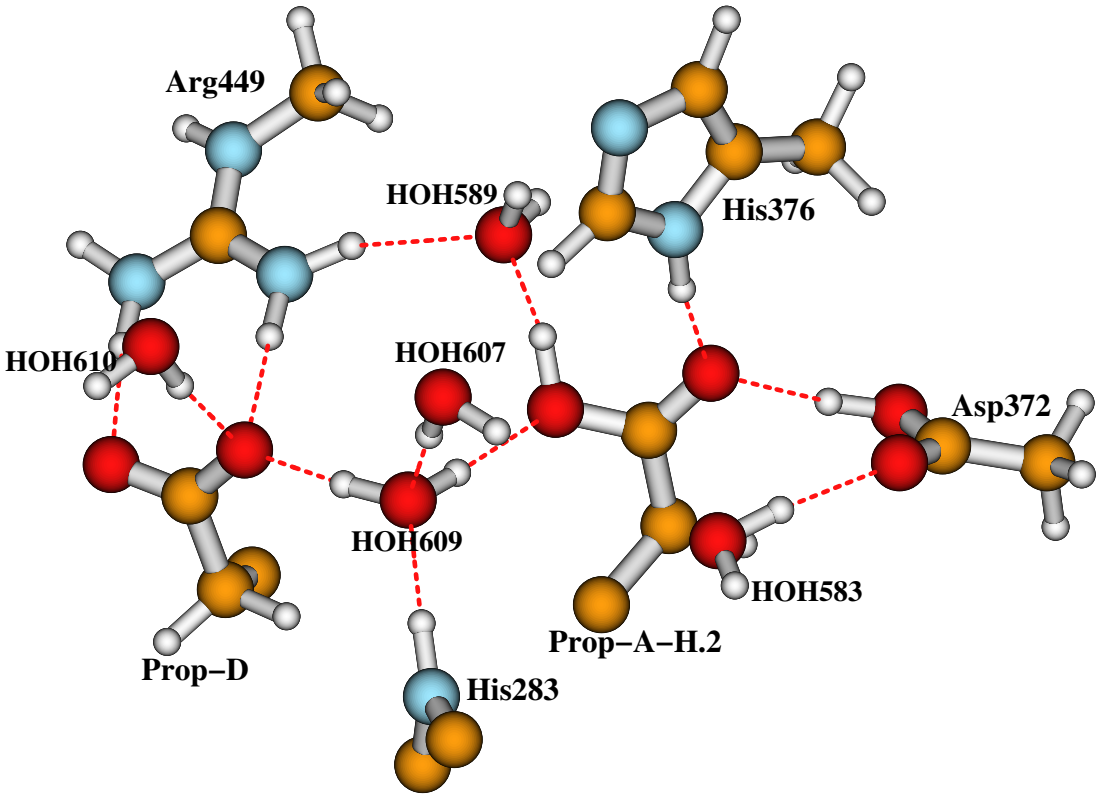

**Table 1.** PW91-D3 and OLYP-D3 Calculated Properties for the Optimized Geometries of $Fe^{3+}$-$(O\text{-}OH)^{-}$-$Cu^{2+}$-$Y237^{-}$ and $Fe^{3+}$-$(HO\text{-}O)^{-}$-$Cu^{2+}$-$Y237^{-}$ DNC Models with or without the "Extra" Proton on His376.[a]

| State | Geometry | | | | *E* | *Q* | p$K_a$ (H376) | Net Spin | | | | |
|---|---|---|---|---|---|---|---|---|---|---|---|---|
| | Fe-O1 | O1-O2 | Cu-O2 | Fe···Cu | | | | $Fe_{a3}$ | $Cu_B$ | O1 | O2 | Y237 |
| **PW91-D3**: | | | | | | | | | | | | |
| $Fe^{3+}$-$(O\text{-}OH)^{-}$-$Cu^{2+}$-$Y237^{-}$-H376 | 1.78 | 1.53 | 2.08 | 4.36 | 2.2 | 0 | | 0.81 | –0.37 | 0.15 | –0.06 | –0.33 |
| $Fe^{3+}$-$(O\text{-}OH)^{-}$-$Cu^{2+}$-$Y237^{-}$-$H376^{+}$ | 1.78 | 1.53 | 2.10 | 4.38 | 0.0 | 1 | 11.2 | 0.81 | –0.37 | 0.15 | –0.06 | –0.34 |
| $Fe^{3+}$-$(HO\text{-}O)^{-}$-$Cu^{2+}$-$Y237^{-}$-H376 | 2.01 | 1.46 | 1.94 | 4.30 | 13.6 | 0 | | 0.74 | –0.47 | –0.01 | –0.19 | 0.09 |
| $Fe^{3+}$-$(HO\text{-}O)^{-}$-$Cu^{2+}$-$Y237^{-}$-$H376^{+}$ | 2.00 | 1.47 | 1.94 | 4.31 | 10.8 | 1 | 11.7 | 0.84 | –0.41 | 0.00 | –0.14 | –0.15 |
| **OLYP-D3**: | | | | | | | | | | | | |
| $Fe^{3+}$-$(O\text{-}OH)^{-}$-$Cu^{2+}$-$Y237^{-}$-H376 | 1.80 | 1.48 | 2.37 | 4.71 | 0.3 | 0 | | 0.89 | –0.30 | 0.15 | –0.03 | –0.52 |
| $Fe^{3+}$-$(O\text{-}OH)^{-}$-$Cu^{2+}$-$Y237^{-}$-$H376^{+}$ | 1.79 | 1.49 | 2.32 | 4.67 | 0.0 | 1 | 11.0 | 0.89 | –0.30 | 0.15 | –0.03 | –0.52 |
| $Fe^{3+}$-$(HO\text{-}O)^{-}$-$Cu^{2+}$-$Y237^{-}$-H376 | 2.09 | 1.44 | 1.97 | 4.47 | 12.7 | 0 | | 0.78 | –0.44 | –0.03 | –0.25 | 0.12 |
| $Fe^{3+}$-$(HO\text{-}O)^{-}$-$Cu^{2+}$-$Y237^{-}$-$H376^{+}$ | 2.08 | 1.45 | 1.98 | 4.50 | 11.8 | 1 | 11.5 | 0.91 | –0.37 | –0.01 | –0.17 | –0.22 |

[a] The calculated properties include geometries (Å), energies (*E*, offset by –29320.2 kcal $mol^{-1}$ and –28044.7 kcal $mol^{-1}$, respectively, in PW91-D3 and OLYP-D3 calculations), the total charge (Q) of the model cluster, the p$K_a$ values of the His376 side chain, and the Mulliken net spin populations on $Fe_{a3}$, $Cu_B$, O1, O2, and on the heavy atoms of the Tyr237 side chain (the sum total).

**Table 2.** PW91-D3 and OLYP-D3 Calculated Properties for the Optimized Geometries of $Fe^{4+}=O^{2-}\ldots OH^{-}$-$Cu^{2+}$-Y237$^{\bullet}$ and $Fe^{4+}=O^{2-}\cdots HO^{-}$-$Cu^{2+}$-Y237$^{\bullet}$ DNC Models with or without the "Extra" Proton on His376.[a]

| State | Geometry | | | | *E* | *Q* | p$K_a$ (H376) | Net Spin | | | | |
|---|---|---|---|---|---|---|---|---|---|---|---|---|
| | Fe-O1 | O1···O2 | Cu-O2 | Fe···Cu | | | | $Fe_{a3}$ | $Cu_B$ | O1 | O2 | Y237 |
| PW91-D3: | | | | | | | | | | | | |
| $Fe^{4+}=O^{2-}\ldots OH^{-}$-$Cu^{2+}$-Y237$^{\bullet}$-H376 | 1.65 | 2.79 | 1.89 | 4.59 | –0.1 | 0 | | 1.11 | –0.50 | 0.78 | –0.32 | –0.71 |
| $Fe^{4+}=O^{2-}\ldots OH^{-}$-$Cu^{2+}$-Y237$^{\bullet}$-H376$^{+}$ | 1.65 | 2.75 | 1.89 | 4.54 | –3.9 | 1 | 12.4 | 1.11 | –0.50 | 0.78 | –0.32 | –0.71 |
| $Fe^{4+}=O^{2-}\cdots HO^{-}$-$Cu^{2+}$-Y237$^{\bullet}$-H376 | 1.66 | 2.64 | 1.91 | 4.52 | –14.8 | 0 | | 1.25 | –0.52 | 0.75 | –0.17 | –0.89 |
| $Fe^{4+}=O^{2-}\cdots HO^{-}$-$Cu^{2+}$-Y237$^{\bullet}$-H376$^{+}$ | 1.66 | 2.64 | 1.91 | 4.55 | –17.7 | 1 | 11.8 | 1.25 | –0.52 | 0.75 | –0.17 | –0.89 |
| OLYP-D3: | | | | | | | | | | | | |
| $Fe^{4+}=O^{2-}\ldots OH^{-}$-$Cu^{2+}$-Y237$^{\bullet}$-H376 | 1.64 | 3.06 | 1.89 | 4.99 | –10.6 | 0 | | 1.17 | –0.48 | 0.87 | –0.31 | –0.87 |
| $Fe^{4+}=O^{2-}\ldots OH^{-}$-$Cu^{2+}$-Y237$^{\bullet}$-H376$^{+}$ | 1.65 | 3.14 | 1.89 | 5.09 | –12.0 | 1 | 11.8 | 1.17 | –0.48 | 0.88 | –0.30 | –0.90 |
| $Fe^{4+}=O^{2-}\cdots HO^{-}$-$Cu^{2+}$-Y237$^{\bullet}$-H376 | 1.65 | 2.89 | 1.92 | 4.95 | –17.6 | 0 | | 1.25 | –0.51 | 0.82 | –0.23 | –0.93 |
| $Fe^{4+}=O^{2-}\cdots HO^{-}$-$Cu^{2+}$-Y237$^{\bullet}$-H376$^{+}$ | 1.65 | 2.87 | 1.93 | 4.93 | –18.9 | 1 | 11.8 | 1.25 | –0.51 | 0.81 | –0.23 | –0.93 |

[a] The calculated properties include geometries (Å), energies (*E*, offset by –29320.2 kcal mol$^{-1}$ and –28044.7 kcal mol$^{-1}$, respectively, in PW91-D3 and OLYP-D3 calculations), the total charge (Q) of the model cluster, the p$K_a$ values of the His376 side chain, and the Mulliken net spin populations on $Fe_{a3}$, $Cu_B$, O1, O2, and on the heavy atoms of the Tyr237 side chain (the sum total).

**Table 3.** The Relative Energies ($\Delta E$, kcal mol$^{-1}$), Geometric Properties (Å) and Mulliken Net-Spin Populations of the Highest Energy Structures in Figure 5. [a]

| Transition | Highest $\Delta E$ | Geometry | | | Net Spin | | | | |
|---|---|---|---|---|---|---|---|---|---|
| | | Fe-O1 | O1-O2 | Cu-O2 | $Fe_{a3}$ | $Cu_B$ | O1 | O2 | Y237 |
| **PW91-D3**: | | | | | | | | | |
| $Fe^{3+}$-(O-OH)$^{-}$-$Cu^{2+}$-Y237$^{-}$-H376 → $Fe^{4+}$=$O^{2-}$···HO$^{-}$-$Cu^{2+}$-Y237$^{\bullet}$-H376 | 2.4 | 1.68 | 1.76 | 2.02 | 0.81 | –0.37 | 0.25 | –0.11 | –0.35 |
| $Fe^{3+}$-(O-OH)$^{-}$-$Cu^{2+}$-Y237$^{-}$-H376$^{+}$ → $Fe^{4+}$=$O^{2-}$···HO$^{-}$-$Cu^{2+}$-Y237$^{\bullet}$-H376$^{+}$ | 2.6 | 1.69 | 1.73 | 2.03 | 0.80 | –0.36 | 0.24 | –0.11 | –0.36 |
| **OLYP-D3**: | | | | | | | | | |
| $Fe^{3+}$-(O-OH)$^{-}$-$Cu^{2+}$-Y237$^{-}$-H376 → $Fe^{4+}$=$O^{2-}$···HO$^{-}$-$Cu^{2+}$-Y237$^{\bullet}$-H376 | 1.6 | 1.71 | 1.69 | 2.16 | 0.90 | –0.33 | 0.23 | –0.12 | –0.48 |
| $Fe^{3+}$-(O-OH)$^{-}$-$Cu^{2+}$-Y237$^{-}$-H376$^{+}$ → $Fe^{4+}$=$O^{2-}$···HO$^{-}$-$Cu^{2+}$-Y237$^{\bullet}$-H376$^{+}$ | 0.9 | 1.69 | 1.74 | 2.09 | 0.91 | –0.33 | 0.26 | –0.16 | –0.47 |

[a.] Energies are relative to the corresponding optimized $Fe^{3+}$-(O-OH)$^{-}$-$Cu^{2+}$-Y237$^{-}$-H376/H376$^{+}$ structure given in Table 1.

**Table 4.** PW91-D3 and OLYP-D3 Calculated Properties for the $Fe^{3+}$-$(OOH)^{-}$-$Cu^{2+}$-$Y237^{-}$ and $Fe^{4+}=O^{2-}\cdots HO^{-}$-$Cu^{2+}$-$Y237^{\bullet}$ DNC Models with Prop-A being protonated at position 1 or 2 (see Figs. 6 and 7).

| State | Geometry | | | | *E* | *Q* | p$K_a$ (Prop-A) | Net Spin | | | | |
|---|---|---|---|---|---|---|---|---|---|---|---|---|
| | Fe-O1 | O1-O2 | Cu-O2 | Fe⋯Cu | | | | $Fe_{a3}$ | $Cu_B$ | O1 | O2 | Y237 |
| PW91-D3: | | | | | | | | | | | | |
| $Fe^{3+}$-(O-OH)$^{-}$-$Cu^{2+}$-$Y237^{-}$-Prop-A-H.1 | 1.79 | 1.53 | 2.13 | 4.44 | 20.0 | 1 | –3.4 | 0.81 | –0.36 | 0.16 | –0.05 | –0.37 |
| $Fe^{3+}$-(O-OH)$^{-}$-$Cu^{2+}$-$Y237^{-}$-Prop-A-H.2 | 1.78 | 1.54 | 2.11 | 4.41 | 20.8 | 1 | –3.9 | 0.82 | –0.36 | 0.16 | –0.06 | –0.37 |
| $Fe^{4+}=O^{2-}\cdots HO^{-}$-$Cu^{2+}$-$Y237^{\bullet}$-Prop-A-H.1 | 1.66 | 2.64 | 1.91 | 4.55 | 2.0 | 1 | –2.6 | 1.25 | –0.52 | 0.76 | –0.17 | –0.90 |
| $Fe^{4+}=O^{2-}\cdots HO^{-}$-$Cu^{2+}$-$Y237^{\bullet}$-Prop-A-H.2 | 1.66 | 2.64 | 1.91 | 4.53 | 2.0 | 1 | –2.6 | 1.25 | –0.52 | 0.76 | –0.17 | –0.90 |
| OLYP-D3: | | | | | | | | | | | | |
| $Fe^{3+}$-(OOH)$^{-}$-$Cu^{2+}$-$Y237^{-}$-Prop-A-H.1 | 1.79 | 1.49 | 2.34 | 4.68 | 14.8 | 1 | 0.2 | 0.89 | –0.29 | 0.16 | –0.03 | –0.53 |
| $Fe^{3+}$-(OOH)$^{-}$-$Cu^{2+}$-$Y237^{-}$-Prop-A-H.2 | 1.80 | 1.49 | 2.36 | 4.70 | 14.7 | 1 | 0.3 | 0.89 | –0.29 | 0.15 | –0.03 | –0.53 |
| $Fe^{4+}=O^{2-}\cdots HO^{-}$-$Cu^{2+}$-$Y237^{\bullet}$-Prop-A-H.1 | 1.65 | 2.83 | 1.92 | 4.83 | –3.5 | 1 | 0.5 | 1.25 | –0.51 | 0.81 | –0.23 | –0.93 |
| $Fe^{4+}=O^{2-}\cdots HO^{-}$-$Cu^{2+}$-$Y237^{\bullet}$-Prop-A-H.2 | 1.65 | 2.83 | 1.92 | 4.81 | –4.3 | 1 | 1.1 | 1.26 | –0.51 | 0.81 | –0.23 | –0.92 |

[a.] The calculated properties include geometries (Å), energies (*E*, offset by –29320.2 kcal mol$^{-1}$ and –28044.7 kcal mol$^{-1}$, respectively, in PW91-D3 and OLYP-D3 calculations), the total charge (Q) of the model cluster, the p$K_a$ values of Prop-A, and the Mulliken net spin populations on $Fe_{a3}$, $Cu_B$, O1, O2, and on the heavy atoms of the Tyr237 side chain (the sum total).

## References


1. M. Wikström, *Biochim. Biophys. Acta*, 2012, **1817**, 468-475.
2. V. R. I. Kaila, M. I. Verkhovsky and M. Wikström, *Chem. Rev.*, 2010, **110**, 7062-7081.
3. A. A. Konstantinov, *FEBS Lett.*, 2012, **586**, 630-639.
4. C. von Ballmoos, P. Adelroth, R. B. Gennis and P. Brzezinski, *Biochim. Biophys. Acta*, 2012, **1817**, 650-657.
5. S. Iwata, C. Ostermeier, B. Ludwig and H. Michel, *Nature*, 1995, **376**, 660-669.
6. L. Qin, C. Hiser, A. Mulichak, R. M. Garavito and S. Ferguson-Miller, *Proc. Natl. Acad. Sci. U. S. A.*, 2006, **103**, 16117-16122.
7. C. Ostermeier, A. Harrenga, U. Ermler and H. Michel, *Proc. Natl. Acad. Sci. U. S. A.*, 1997, **94**, 10547-10553.
8. T. Tsukihara, H. Aoyama, E. Yamashita, T. Tomizaki, H. Yamaguchi, K. ShinzawaItoh, R. Nakashima, R. Yaono and S. Yoshikawa, *Science*, 1996, **272**, 1136-1144.
9. M. Svensson-Ek, J. Abramson, G. Larsson, S. Tornroth, P. Brzezinski and S. Iwata, *J. Mol. Biol.*, 2002, **321**, 329-339.
10. T. Soulimane, G. Buse, G. P. Bourenkov, H. D. Bartunik, R. Huber and M. E. Than, *EMBO J.*, 2000, **19**, 1766-1776.
11. L. M. Hunsicker-Wang, R. L. Pacoma, Y. Chen, J. A. Fee and C. D. Stout, *Acta Crystallogr. Sect. D. Biol. Crystallogr.*, 2005, **61**, 340-343.
12. J. Koepke, E. Olkhova, H. Angerer, H. Muller, G. H. Peng and H. Michel, *Biochim. Biophys. Acta*, 2009, **1787**, 635-645.
13. H. Aoyama, K. Muramoto, K. Shinzawa-Itoh, K. Hirata, E. Yamashita, T. Tsukihara, T. Ogura and S. Yoshikawa, *Proc. Natl. Acad. Sci. U. S. A.*, 2009, **106**, 2165-2169.
14. B. Liu, Y. Chen, T. Doukov, S. M. Soltis, C. D. Stout and J. A. Fee, *Biochemistry*, 2009, **48**, 820-826.
15. T. Tiefenbrunn, W. Liu, Y. Chen, V. Katritch, C. D. Stout, J. A. Fee and V. Cherezov, *Plos One*, 2011, **6**, e22348.
16. O. Farver, Y. Chen, J. A. Fee and I. Pecht, *FEBS Lett.*, 2006, **580**, 3417-3421.
17. J. A. Fee, D. A. Case and L. Noodleman, *J. Am. Chem. Soc.*, 2008, **130**, 15002-15021.
18. V. M. Luna, Y. Chen, J. A. Fee and C. D. Stout, *Biochemistry*, 2008, **47**, 4657-4665.
19. B. Schmidt, J. McCracken and S. Ferguson-Miller, *Proc. Natl. Acad. Sci. U. S. A.*, 2003, **100**, 15539-15542.

20. C. Varotsis, W. H. Woodruff and G. T. Babcock, *J. Biol. Chem.*, 1990, **265**, 11131-11136.
21. S. H. Han, Y. C. Ching and D. L. Rousseau, *Biochemistry*, 1990, **29**, 1380-1384.
22. S. Yoshikawa and A. Shimada, *Chem. Rev.*, 2015, **115**, 1936-1989.
23. O. Einarsdottir, *Biochim. Biophys. Acta*, 1995, **1229**, 129-147.
24. M. Wikström, *Proc. Natl. Acad. Sci. U. S. A.*, 1981, **78**, 4051-4054.
25. L. C. Weng and G. M. Baker, *Biochemistry*, 1991, **30**, 5727-5733.
26. J. E. Morgan, M. I. Verkhovsky and M. Wikstrom, *Biochemistry*, 1996, **35**, 12235-12240.
27. D. A. Proshlyakov, M. A. Pressler and G. T. Babcock, *Proc. Natl. Acad. Sci. U. S. A.*, 1998, **95**, 8020-8025.
28. M. Fabian, W. W. Wong, R. B. Gennis and G. Palmer, *Proc. Natl. Acad. Sci. U. S. A.*, 1999, **96**, 13114-13117.
29. G. T. Babcock, *Proc. Natl. Acad. Sci. U. S. A.*, 1999, **96**, 12971-12973.
30. D. A. Proshlyakov, M. A. Pressler, C. DeMaso, J. F. Leykam, D. L. DeWitt and G. T. Babcock, *Science*, 2000, **290**, 1588-1591.
31. E. A. Gorbikova, I. Belevich, M. Wikstrom and M. I. Verkhovsky, *Proc. Natl. Acad. Sci. U. S. A.*, 2008, **105**, 10733-10737.
32. Z. Halime, M. T. Kieber-Emmons, M. F. Qayyum, B. Mondal, T. Gandhi, S. C. Puiu, E. E. Chufan, A. A. N. Sarjeant, K. O. Hodgson, B. Hedman, E. I. Solomon and K. D. Karlin, *Inorg. Chem.*, 2010, **49**, 3629-3645.
33. M. T. Kieber-Emmons, Y. Q. Li, Z. Halime, K. D. Karlin and E. I. Solomon, *Inorg. Chem.*, 2011, **50**, 11777-11786.
34. M. T. Kieber-Emmons, M. F. Qayyum, Y. Q. Li, Z. Halime, K. O. Hodgson, B. Hedman, K. D. Karlin and E. I. Solomon, *Angew. Chem. Int. Ed.*, 2012, **51**, 168-172.
35. I. Garcia-Bosch, S. M. Adam, A. W. Schaefer, S. K. Sharma, R. L. Peterson, E. I. Solomon and K. D. Karlin, *J. Am. Chem. Soc.*, 2015, **137**, 1032-1035.
36. Y. Yoshioka, H. Satoh and M. Mitani, *J. Inorg. Biochem.*, 2007, **101**, 1410-1427.
37. Y. Yoshioka and M. Mitani, *Bioinorganic Chemistry and Applications*, 2010, 182804.
38. M. R. A. Blomberg, P. E. M. Siegbahn, G. T. Babcock and M. Wikstrom, *J. Am. Chem. Soc.*, 2000, **122**, 12848-12858.
39. M. R. A. Blomberg, P. E. M. Siegbahn and M. Wikström, *Inorg. Chem.*, 2003, **42**, 5231-5243.

40. L. Noodleman, W.-G. Han Du, J. A. Fee, A. W. Götz and R. C. Walker, *Inorg. Chem.*, 2014, **53**, 6458-6472.
41. A. D. Becke, *Phys. Rev. A*, 1988, **38**, 3098-3100.
42. A. D. Becke, *J. Chem. Phys.*, 1993, **98**, 1372-1377.
43. A. D. Becke, *J. Chem. Phys.*, 1993, **98**, 5648-5652.
44. J. P. Perdew, J. A. Chevary, S. H. Vosko, K. A. Jackson, M. R. Pederson, D. J. Singh and C. Fiolhais, *Phys. Rev. B*, 1992, **46**, 6671-6687.
45. N. C. Handy and A. J. Cohen, *Mol. Phys.*, 2001, **99**, 403-412.
46. C. T. Lee, W. T. Yang and R. G. Parr, *Phys. Rev. B*, 1988, **37**, 785-789.
47. S. Grimme, J. Antony, S. Ehrlich and H. Krieg, *J. Chem. Phys.*, 2010, **132**, 154104.
48. I. Szundi, C. Funatogawa, J. A. Fee, T. Soulimane and O. Einarsdottir, *Proc. Natl. Acad. Sci. U. S. A.*, 2010, **107**, 21010-21015.
49. V. R. I. Kaila, V. Sharma and M. Wikstrom, *Biochimica Et Biophysica Acta-Bioenergetics*, 2011, **1807**, 80-84.
50. W.-G. Han Du and L. Noodleman, *Inorg. Chem.*, 2013, **52**, 14072-14088.
51. S. Vancoillie, H. L. Zhao, M. Radon and K. Pierloot, *J. Chem. Theory Comput.*, 2010, **6**, 576-582.
52. M. Radoń and K. Pierloot, *J. Phys. Chem. A*, 2008, **112**, 11824-11832.
53. W.-G. Han Du and L. Noodleman, *Inorg. Chem.*, 2015, **54**, 7272-7290.
54. ADF, *Amsterdam Density Functional Software*, SCM, Theoretical Chemistry, Vrije Universiteit, Amsterdam, The Netherlands. http://www.scm.com.
55. G. te Velde, F. M. Bickelhaupt, E. J. Baerends, C. F. Guerra, S. J. A. Van Gisbergen, J. G. Snijders and T. Ziegler, *J. Comput. Chem.*, 2001, **22**, 931-967.
56. C. F. Guerra, O. Visser, J. G. Snijders, G. te Velde and E. J. Baerends, in *Methods and techniques for computational chemistry*, eds. E. Clementi and C. Corongiu, STEF, Cagliari, 1995, pp. 303-395.
57. A. Klamt and G. Schüürmann, *J. Chem. Soc., Perkin Trans. 2*, 1993, 799-805.
58. A. Klamt, *J. Phys. Chem.*, 1995, **99**, 2224-2235.
59. A. Klamt and V. Jonas, *J. Chem. Phys.*, 1996, **105**, 9972-9981.
60. C. C. Pye and T. Ziegler, *Theor. Chem. Acc.*, 1999, **101**, 396-408.
61. L. Noodleman, *J. Chem. Phys.*, 1981, **74**, 5737-5743.
62. L. Noodleman and D. A. Case, *Adv. Inorg. Chem.*, 1992, **38**, 423-470.

63. L. Noodleman, T. Lovell, W.-G. Han, T. Liu, R. A. Torres and F. Himo, in *Comprehensive Coordination Chemistry II, From Biology to Nanotechnology*, ed. A. B. Lever, Elsevier Ltd, 2003, vol. 2, pp. 491-510.
64. M. D. Tissandier, K. A. Cowen, W. Y. Feng, E. Gundlach, M. H. Cohen, A. D. Earhart, J. V. Coe and T. R. Tuttle, *J. Phys. Chem. A*, 1998, **102**, 7787-7794.
65. D. G. Truhlar, C. J. Cramer, A. Lewis and J. A. Bumpus, *J. Chem. Educ.*, 2004, **81**, 596-604.
66. D. G. Truhlar, C. J. Cramer, A. Lewis and J. A. Bumpus, *J. Chem. Educ.*, 2007, **84**, 934.
67. A. V. Marenich, J. M. Ho, M. L. Coote, C. J. Cramer and D. G. Truhlar, *PCCP*, 2014, **16**, 15068-15106.
68. G. J. Tawa, I. A. Topol, S. K. Burt, R. A. Caldwell and A. A. Rashin, *J. Chem. Phys.*, 1998, **109**, 4852-4863.
69. G. M. Fleck, *Chemical reaction mechanisms*, Holt, Rinehart and Winston, Inc., 1971.
70. C. von Ballmoos, N. Gonska, P. Lachmann, R. B. Gennis, P. Adelroth and P. Brzezinski, *Proc. Natl. Acad. Sci. U. S. A.*, 2015, **112**, 3397-3402.
71. H. Y. Chang, S. K. Choi, A. S. Vakkasoglu, Y. Chen, J. Hemp, J. A. Fee and R. B. Gennis, *Proc. Natl. Acad. Sci. U. S. A.*, 2012, **109**, 5259-5264.